JACS
JOURNAL OF THE AMERICAN CHEMICAL SOCIETY
Article
pubs.acs.org/JACS

Rational Design of Chiral Nanostructures from Self-Assembly of a Ferrocene-Modified Dipeptide

Yuefei Wang,[†] Wei Qi,*[,†,§,∥] Renliang Huang,[‡] Xuejiao Yang,[†] Mengfan Wang,[†,∥] Rongxin Su,[†,§,∥] and Zhimin He[†]

[†]State Key Laboratory of Chemical Engineering, School of Chemical Engineering and Technology and [‡]School of Environmental Science and Engineering, Tianjin University, Tianjin 300072, PR China

[§]Collaborative Innovation Center of Chemical Science and Engineering (Tianjin), Tianjin 300072, PR China

[∥]Tianjin Key Laboratory of Membrane Science and Desalination Technology, Tianjin 300072, PR China

Supporting Information

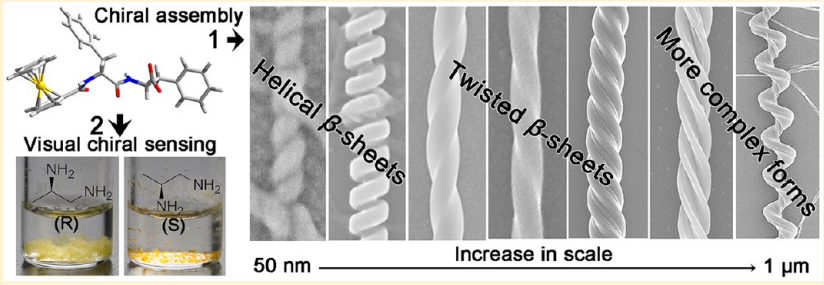

ABSTRACT: We report a new paradigm for the rational design of chiral nanostructures that is based on the hierarchical self-assembly of a ferrocene (Fc)-modified dipeptide, ferrocene-L-Phe-L-Phe-OH (Fc-FF). Compared to other chiral self-assembling systems, Fc-FF is unique because of its smaller size, biocompatibility, multiple functions (a redox center), and environmental responsiveness. X-ray and spectroscopic analyses showed that the incorporation of counterions during the hierarchical self-assembly of Fc-FF changed the conformations of the secondary structures from flat β sheets into twisted β sheets. This approach enables chiral self-assembly and the formation of well-defined chiral nanostructures composed of helical twisted β sheets. We identified two elementary forms for the helical twist of the β sheets, which allowed us to create a rich variety of rigid chiral nanostructures over a wide range of scales. Furthermore, through subtle modulations in the counterions, temperature, and solvent, we are able to precisely control the helical pitch, diameter, and handedness of the self-assembled chiral nanostructures. This unprecedented level of control not only offers insights into how rationally designed chiral nanostructures can be formed from simple molecular building blocks but also is of significant practical value for the use in chiroptics, templates, chiral sensing, and separations.

INTRODUCTION

The rational design of chiral nanostructures with precise control is a fascinating topic in chemistry and materials science and has practical ramifications in many fields, such as chiroptics,[1−3] templates,[4,5] chiral sensing,[6−8] and separation.[9−11] Such a synthetic advancement requires a fundamental understanding of the underlying processes. For the self-assembly of amphiphilic lipids[12] and liquid crystals,[13] the formation of chiral nanostructures and their structural control can be achieved by manipulating the competition between local chiral interactions and global geometric constraints imposed by the self-assembled structures. In this process, the main challenges lie in the difficulty of precisely tailoring the complex balance between noncovalent forces and the stepwise amplification of the molecular chirality at different stages in the hierarchical process.

Self-assembly from biologically relevant molecules (e.g., peptides and DNA) represents a general strategy for the construction of well-defined chiral nanostructures. In the field of amyloid fibrillization, a wide variety of proteins or amyloid polypeptides have been shown to self-assemble into twisted nanofibrils or helical ribbons.[14−23] These chiral nanostructures are generally characterized by a set of 1D twisted β sheets ("cross β" spines) running along the axis of the fiber.[24,25] This result indicates that the formation of chiral secondary structures, such as twisted β sheets, might be an important step toward the expression of molecular chirality on the nano- or microscale. However, the development of a rational approach for the design of rigid chiral nanostructures from the self-assembly of much simpler or shorter peptides remains a formidable challenge. Peptides with fewer sequences prefer to self-assemble into flat β sheets because of their weak molecular chirality, which can be easily offset by adjusting the molecular

Received: April 16, 2015
Published: May 27, 2015

DOI: 10.1021/jacs.5b03925
J. Am. Chem. Soc. 2015, 137, 7869−7880

conformation. For example, Eisenberg et al. identified a series of peptides (4−7 residues) with different "steric zipper" β-sheet arrangements, and all of them were flat β sheets.[26,27] Similar phenomena were also observed for a class of dipeptides.[28,29] Such "achiral" secondary molecular arrangements of peptides hinder the further translation of molecular chirality to a larger scale. Indeed, self-assembly of well-defined chiral nanostructures from simple peptide molecular building blocks has been only demonstrated in rare cases within the corpus of peptide fibrillization.[30−36]

The diphenylalanine peptide (L-Phe-L-Phe, FF),[37] which is extracted from the Alzheimer's β-amyloid polypeptide, has attracted considerable attention because of its biological significance, chemical simplicity, and excellent capacity to form a wide range of nanostructures. Since the seminal works of Görbitz et al. and Gazit et al., FF has been shown to form nanotubes,[37] nanowires,[38,39] nanoarrays,[40,41] nanospheres,[42,43] and microtubes.[44] The interesting mechanical[45] and physical[46,47] properties of these materials are advantageous for biocompatible nanomaterials with applications in various fields, including as templates,[37] piezoelectronics,[46] optics,[48] and biosensors.[49] Moreover, modification at the amino terminus of FF with fluorenylmethoxycarbonyl (Fmoc),[50,51] naphthalene (Nap),[52] or *p*-borono-phenylmethoxy carbonyl (BPmoc)[53] functionalities further imparts FF with novel functions, such as pH- and redox-responsive self-assembly. However, until now, chiral self-assembly based on FF has not been reported, although it is composed of two chiral phenylalanine residues. The integration of chiral interactions during the hierarchical self-assembly of FF may be an attractive paradigm for the rational design of chiral nanostructures, if this process can be regulated precisely.

In our previous work, we discovered that the ferrocene-modified derivative of FF, ferrocene-L-Phe-L-Phe-OH (Fc-FF), could self-assemble into a stable, redox-responsive hydrogel under kinetic control.[54,55] Here, we report that the precise expression of molecular chirality during the hierarchical self-assembly of Fc-FF allowed us to create a wide variety of chiral nanostructures with unprecedented levels of diversity and precision (Scheme 1). By virtue of the core recognition motif of FF and the irregular shape of the Fc moiety, Fc-FF was a rather intractable molecule building block. Many variables (e.g., counterions, pH, temperature, and solvent) play crucial roles in directing the chiral self-assembly of Fc-FF. Therefore, very subtle modulations in conditions precisely controlled the degree of twisting (helical pitch), the diameter, and the handedness of the self-assembled chiral nanostructures. This unprecedented level of control will significantly enhance the relevance of peptide-based materials in a broad spectrum of applications, i.e., serving as probes for chiral sensing or templates to fabricate other chiral nanomaterials.

RESULTS AND DISCUSSION

General Strategies for the Rational Design of Chiral Nanostructures. Our strategy for the rational design of chiral nanostructures was based on the idea that the emergence of chiral nanostructures can be achieved via the precise control of the helical twist of the β sheets in different stages of the peptide self-assembly. This process requires a delicate balance among the chiral interactions, the noncovalent driving forces, and the related geometric constraints. Here, we identified three facile strategies to control the chiral organization of Fc-FF, as follows: (1) Counterions mutate the secondary structure of Fc-FF into twisted β sheets via strong hydrogen bonding and electrostatic interactions at the C terminus of the peptide. Counterions can also be used to control the chiral interactions between individual twisted β sheets by changing the rigidity of the counterions. (2) Temperature is closely related to the self-assembly speed. The helical twist of the β sheets is a kinetically controlled process, which requires a fast self-assembling speed corresponding to higher temperatures. Temperature can also be used to balance the competition between the chiral interactions and the geometric constraints, which allows us to precisely control the diameter and helical pitch of the self-assembled chiral nanostructures. (3) Solvent has a significant influence on the complex balance of the noncovalent driving forces between molecular building blocks and can thus be used to control the self-assembly of hierarchical chiral nanostructures.

Scheme 1. Proposed Schematic Illustration Showing the Hierarchical, Chiral Self-Assembly of Ferrocene-L-Phe-L-Phe-OH (Fc-FF) into Rationally Designed Chiral Nanostructures[a,b,c,d]

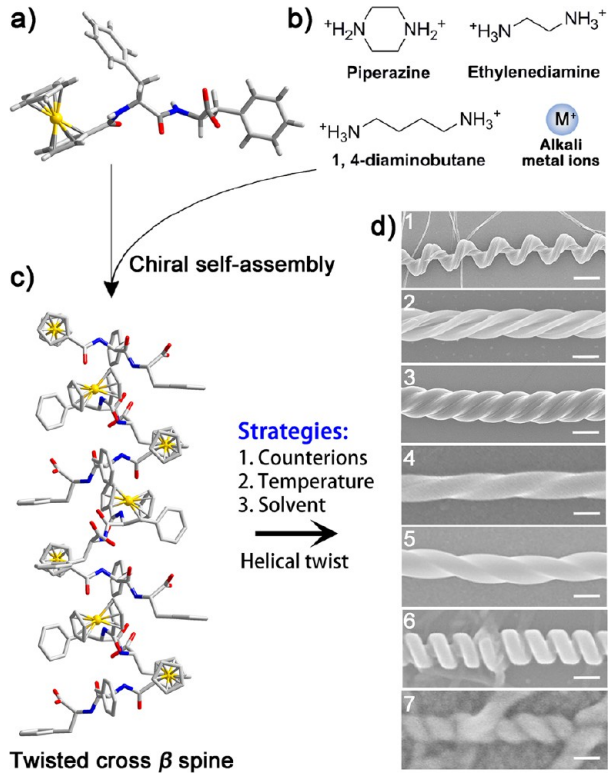

[a]Molecular structure of Fc-FF from the single crystal structure determination (grey: carbon, red: oxygen, blue: nitrogen, white: hydrogen). [b]Counterions used to direct the chiral self-assembly of Fc-FF. [c]Single-crystal structure of Fc-FF showing the cross β spine of a twisted β sheet in Fc-FF. [d]Rationally designed hierarchical chiral nanostructures with unprecedented levels of diversity and precision (top-down): (1) nanoscrews (scale bar = 1 μm), (2) nanohelices formed via the twist of two crossed ribbons (scale bar = 300 nm), (3) big twists (scale bar = 200 nm), (4 and 5) left- or right-handed, respectively, twisted ribbons (scale bar = 100 nm), (6) rigid nanosprings (scale bar = 100 nm), (7) tubelike helical ribbons (scale bar = 50 nm). Chiral nanostructures in d1−5 were self-assembled with piperazine counterions via precise control of the temperatures, solvents and pH. The rigid nanosprings in d6 were grown with ethylenediame or 1,4-diaminobutane in less polar solvents. The tubelike helical ribbons in d7 were self-assembled in the presence of alkali metal ions (Na^+ or K^+) in less polar solvents.

DOI: 10.1021/jacs.5b03925
J. Am. Chem. Soc. 2015, 137, 7869−7880

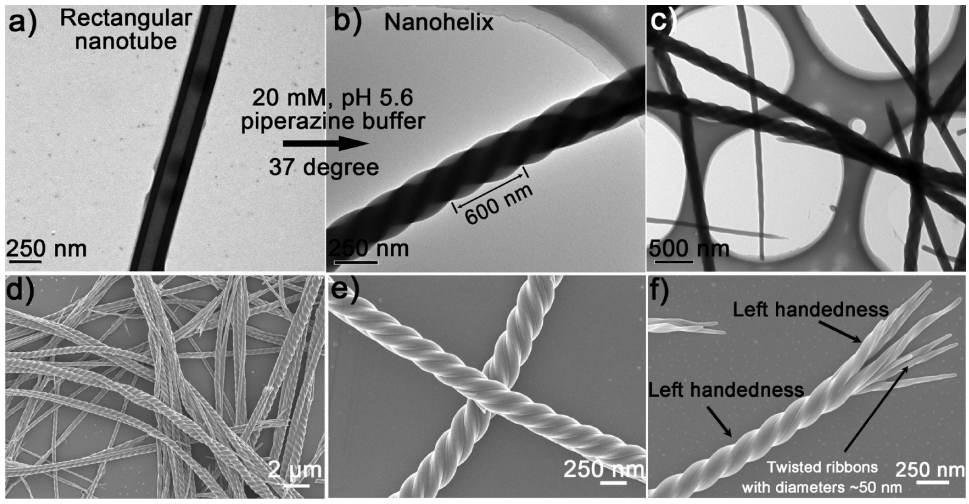

Figure 1. (a) Transmission electron microscope (TEM) image of the rectangular nanotubes formed by the hierarchical self-assembly of ferrocene-diphenylalanine (Fc-FF) in 10% HFIP/90% H_2O at 20 °C. (b and c) Low- and high-magnification TEM images of the elegant nanohelices formed by the chiral self-assembly of Fc-FF in 10% HFIP/90% piperazine buffer solution (20 mM, pH 5.6) at 37 °C. (d and e) Low- and high-magnification scanning electron microscopy (SEM) images of the twisted Fc-FF nanohelices in 10% HFIP/90% piperazine buffer solution (20 mM, pH 5.6) at 37 °C. (f) High-magnification SEM images showing that the left-handed nanohelices were formed by the chiral twist of thinner Fc-FF nanohelices with the same handedness.

Strategy 1: Counterion-Directed, Chiral Self-Assembly of Elegant Big Twists. As the first step toward the rational design of chiral nanostructures, we selected piperazine, a six-membered heterocyclic counterion, to direct the chiral self-assembly of Fc-FF. In a typical experiment, lyophilized Fc-FF powder was dissolved in 1,1,1,3,3,3-hexafluoro-2-propanol (HFIP), a highly polar solvent, at a concentration of 40 mM. The Fc-FF HFIP solution (100 μL) was then injected into a piperazine buffer solution (900 μL, 20 mM, pH 5.6) to yield a mixture of 10% HFIP and 90% H_2O (v/v) with 4 mM Fc-FF. The turbid yellow suspension was incubated at 37 °C for 2 h without any disturbance, during time which large amounts of fibers were formed. As a control experiment, the self-assembly of Fc-FF without piperazine was also performed following a similar procedure. The fibers grew much faster in the samples with piperazine counterions than those without them, indicating that the counterions promote the aggregation and self-assembly of Fc-FF. Transmission electron microscopy (TEM) and scanning electron microscopy (SEM) were used to investigate the influence of counterions on the self-assembled structures. As shown in Figure 1a, well-defined rectangular nanotubes were formed by Fc-FF alone. Surprisingly, large amounts of left-handed nanohelices were assembled at 37 °C in the presence of piperazine counterions (Figure 1b). The self-assembled Fc-FF nanohelices were rigid and had diameters of ~250 nm, helical pitches of ~600 nm (Figure 1b,c), and lengths up to hundreds of micrometers. The large-area SEM image demonstrated that the Fc-FF nanohelices were highly homogeneous, and no other assemblages were observed (Figure 1d). High-magnification SEM images revealed that the well-defined, left-handed nanohelices were formed from the helical twist of large bundles of twisted ribbons with the same handedness (Figure 1e,f), reminiscent of the "big twists" specialty food in Tianjin, China. The hierarchical structure of the big twists reflected a stepwise amplification of molecular chirality during the self-assembly of Fc-FF. Moreover, if we used the D-amino-acid analog of the peptide, ferrocene-D-Phe-D-Phe-OH, then elegant big twists with the same structural features but with right-handedness were observed (Figure S1), indicating the intrinsic chiral organization of peptides at the molecular scale.

To gain insight into the secondary structure of the Fc-FF nanostructures, circular dichroism (CD) spectroscopy and Fourier transform infrared (FT-IR) spectroscopy were performed. With regard to CD analysis (Figure 2a), the rectangular nanotubes were completely CD silent in the spectral range, whereas the Fc-FF big twists had a strong exciton−couplet Cotton effect in the peptide region with a maximum at 200 nm and a minimum at 224 nm, which could be associated with the twisted β sheets.[35,56] Another strong exciton−couplet Cotton effect was observed in the aromatic region, with a negative peak centered at 266 nm and three positive peaks at 296, 322 and 355 nm. The emergence of a couplet Cotton effect is typically associated with strong $\pi-\pi$ stacking between the chromophores. The results above indicate that both the Fc moiety and aromatic rings in the big twists are associated with strong $\pi-\pi$ stacking and involved in a highly asymmetric environment because of the strong twists of the peptide β sheets. Moreover, CD signals also appeared at higher wavelengths for the big twists. These signals could be assigned to the chiral scattering of light as a result of the interaction of the light with the chiral nanostructures.[6]

With regard to IR analysis (Figure 2b), the rectangular nanotubes had strong adsorption peaks at 1632 and 1667 cm^{-1}, which could be assigned to antiparallel β sheet structures.[57] We also observed two adsorption peaks at 1768 and 1739 cm^{-1}, assigned to the carbonyl group at the C terminus of Fc-FF. The dual adsorption in this region and their relatively strong intensities indicate that the carbonyl groups in the rectangular nanotubes were likely involved with different forms of weak hydrogen bonds. However, the big twists only showed a very weak adsorption at approximately 1733 cm^{-1} in this region. These results suggest the hydrogen bonds assigned to the carboxylic groups were much stronger in the big twists than in the nanotubes, possibly because of the formation of strong extended hydrogen bonds between the Fc-FF peptides and the piperazine counterions. Moreover, the adsorption peaks at 1630 cm^{-1} indicate that the big twists also had β-sheet arrangements.

DOI: 10.1021/jacs.5b03925
J. Am. Chem. Soc. 2015, 137, 7869−7880

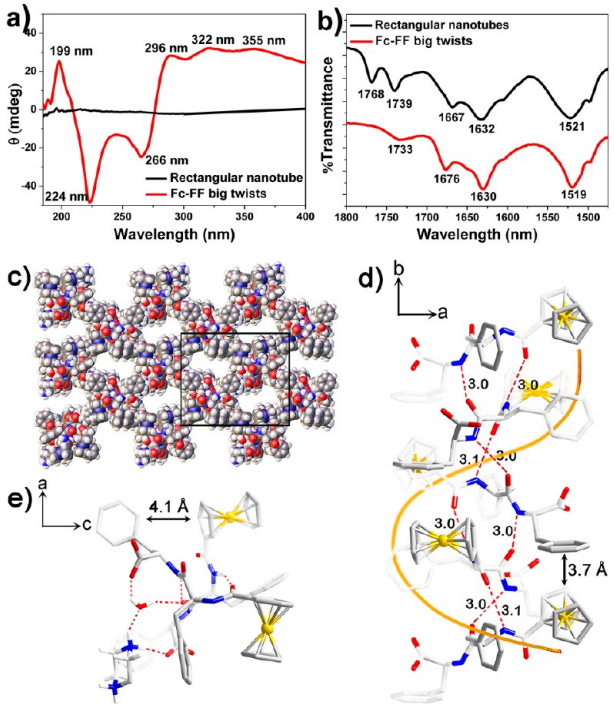

Figure 2. (a and b) Circular dichroism (CD) and Fourier transform infrared (FT-IR) spectra of the rectangular nanotubes (black curve) and big twists (red curve). (c) Single crystal structure of Fc-FF with a porous architecture. The atoms are shown as spheres representing van der Waals radii (gray, carbon; red, oxygen; blue, nitrogen; white, hydrogen). (d) Close-up view of the twisted β sheet from the side (down the c axis) showing five Fc-FF β strands rotated ~90° clockwise around the b axis through hydrogen bonds and $\pi-\pi$ stacking. Peptide backbone hydrogen bonds are shown by red dots. Hydrogen bond lengths are noted in angstroms. The $\pi-\pi$ stacking between the Fc moiety and the aromatic ring is indicated by the black arrow spaced by a distance of 3.7 Å. (e) Fc-FF dimers viewed down the b axis, showing the helical organization of the two Fc-FF molecules stabilized by a piperazine counterion and a water molecule through hydrogen bonds.

However, the deviations in the peak locations between the nanotubes (1667, 1632, and 1521 cm^{-1}) and the big twists (1676, 1630, and 1519 cm^{-1}) in the amide adsorption regions indicate a slight change in the hydrogen bonding between the peptides in the two nanostructures.

To obtain further structural information, we produced a single crystal of Fc-FF, suitable for X-ray crystallographic analysis, that was grown by slow diffusion of the piperazine aqueous solution into the HFIP solution of Fc-FF. The single-crystal structure (Figure 2c) showed a porous architecture and clearly displayed a 1D cross β spine, which was a twisted β sheet of Fc-FF with left-handedness (Figure 2d). Each Fc-FF β strand in the sheet rotated ~90° clockwise around the fiber axis and extended via hydrogen bonding and $\pi-\pi$ stacking (Figures 2d and S2). The elementary structure of the crystal was a helical Fc-FF dimer stabilized by a counterion and a water molecule at the C termini of the peptides (Figure 2e), suggesting that the counterion can serve as a holder to stabilize the helical architecture of the β sheets via strong hydrogen bonding and electrostatic interactions. The stacking between two neighboring β sheets was primarily driven by the $\pi-\pi$ stacking between the aromatic rings and the Fc moieties in two sheets and the hydrogen bonds between the peptides and the embedded counterions and water molecules (Figures S3–S5).

Powder X-ray diffraction (Figure S6) was used to compare the structural motif of the single crystal with the self-assembled rectangular nanotubes and big twists. As shown in Figure S6, both the rectangular nanotubes and the big twists had diffraction peaks at 2θ values of 24, 22.2, and 20.6°, corresponding to d spacings of 3.7, 4.0, and 4.3 Å, respectively. The d spacings of 3.7 and 4.0 Å could be assigned to the strong $\pi-\pi$ stacking interactions, and 4.3 Å was attributed to the spacing between peptides within the β sheet structure. Moreover, the big twists had reflection peaks corresponding to d spacings of 1.52, 1.07, and 1.0 nm. These values are consistent with the dimension of the twisted β sheets within the single crystal (Figure S3). The rectangular nanotubes showed disparate reflections, suggesting a different β-sheet arrangement than that of the single crystal.

The spectroscopic measurements and X-ray analysis demonstrate that the incorporation of counterions changed the conformation of the secondary structures from antiparallel β sheets (flat β sheets) to highly twisted β sheets. On the basis of this observation, the big twists were formed via the hierarchical helical twisting of the β sheets, and the rectangular nanotubes were formed via the parallel stacking of the flat β sheets. The formation of strong hydrogen bonds and electrostatic interactions between the counterions and the C termini of the peptides is essential for the change in secondary structures and the formation of well-defined chiral nanostructures. As demonstrated in Figure S7, highly twisted chiral nanostructures with intense CD signals were only formed within a specific pH range (pH 5.3–5.6). At lower pH values (pH < 5.0), Fc-FF self-assembled into rectangular nanotubes rather than big twists (Figure S7c). At higher pH values (pH > 6.0), Fc-FF self-assembled into heterogeneous chiral nanostructures (Figure S7f), which were semistable and transformed into yellow crystals after 24 h of incubation (Figure S7g). The pH is closely related to the zeta potential of the charged aggregates in solution and therefore, in this case, determines the electrostatic interactions between the counterions and the peptide aggregates.

To gain further insights into this counterion-directed strategy, we tested a series of counterions with distinct structural features and investigated their influences on the chiral self-assembly of Fc-FF (Table 1). We defined the counterions as "rigid" or "soft" on the basis of their affinity for the C termini of the peptides and the flexibility of the molecular

Table 1. Direction of Chiral Self-Assembly of Fc-FF by Using Different Counterions[a]

entry	counterions[b]	HFIP/H_2O	Diameter
1		(L)-big twists	200-300 nm
2	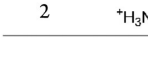	(R)-nanohelices	100-200 nm
3		Amorphous aggregates	--
4	Na^+ or K^+	Platelet microtubes	> 1 μm

[a]All experiments were performed at 37 °C in 10% HFIP and 90% H_2O. [b]Counterion solutions were prepared by dissolving the corresponding components in ddH_2O at 20 or 100 mM, titrated to pH 5.6 at 20 °C.

DOI: 10.1021/jacs.5b03925
J. Am. Chem. Soc. 2015, 137, 7869–7880

structure. For example, both piperazine and ethylenediamine could form strong hydrogen bonds and electrostatic interactions with Fc-FF. However, piperazine is a six-membered heterocyclic counterion and, therefore, is much more rigid than the linear counterion ethylenediamine. Furthermore, the alkali metal ions are much softer counterions because of their weak electrostatic interactions with the C termini of peptides. On the basis of these points, a qualitative sequence of counterion rigidity follows: piperazine > ethylenediamine >1,4-diaminobutane > Na^+ or K^+. Counterion rigidity significantly influenced the chiral self-assembly of Fc-FF, which allowed us to fabricate chiral nanostructures with distinct architectures. For example, in the presence of ethylenediamine, which had a softer molecular conformation compared with that of piperazine, Fc-FF self-assembled into right-handed chiral nanostructures with diameters of ~100 nm (Figure S8a). A higher magnification SEM image revealed that the right-handed chiral nanostructures were composed of flexible right-handed twisted ribbons (Figure S8b). Moreover, CD analysis revealed distinct Cotton effects from those of the big twists, indicating a dramatic change in the secondary structure (Figure S8d). Intriguingly, when we used 1,4-diaminobutane, a much softer counterion with an even longer alkyl chain, Fc-FF formed amorphous aggregates without any supramolecular chirality (Figure S8c,d) rather than chiral nanostructures. A possible interpretation for this may lie in the flexibility of 1,4-diaminobutane, which lacks the required rigidity to support the 3D framework of the self-assembled supramolecular structures. Moreover, when we used alkali metal ions, such as Na^+ and K^+, Fc-FF self-assembled into rectangular microtubes (Figure S9). Such soft counterions simply cannot drive the chiral self-assembly of Fc-FF in highly polar solvents because of their low affinity for the C termini of peptides. However, attractive chiral self-assembly was observed if a less polar solvent was used, which will be addressed later.

Strategy 2: Kinetic Control (Temperature) Drives the Formation of Well-Defined Chiral Nanostructures with Finite Diameters and Precisely Tailored Helical Pitches. In addition to the incorporation of counterions, the subtle modulation of temperature allowed us to control the chiral nanostructures at much higher levels of precision. To determine the importance of the temperature in the direction of the chiral self-assembly of Fc-FF, we prepared big twists at different temperatures. SEM analysis revealed that Fc-FF self-assembled into dendritic microcrystals composed of very thick microbelts at T < 30 °C (Figure S10a,b). Stable big twists were formed at T > 37 °C (Figure S10c–f). CD analysis revealed that the dendritic microcrystals were completely CD-silent (Figure 3a), whereas intense CD signals were detected for the big twists. We plotted the CD intensities at 322 nm as a function of temperature (Figure 3b), from which we could define two important temperature values: T_c at 30 °C, for the emergence of chiral nanostructures, and T_m at 37 °C, the optimal temperature for chiral self-assembly. At $T < T_c$ (chiral-silent region), Fc-FF self-assembled into platelet nanostructures, and at $T > T_m$ (chiral-amplification region), Fc-FF self-assembled into big twists. Intriguingly, when self-assembly developed in the region from T_c to T_m (semistable region), Fc-FF initially formed big twists that were unstable and transformed into large crystals after 48 h of incubation (Figure S11). The big twists were very stable when incubated at T > 37 °C but become unstable at T < 37 °C and would spontaneously transform into single crystals (Figure 3c). Moreover, if we

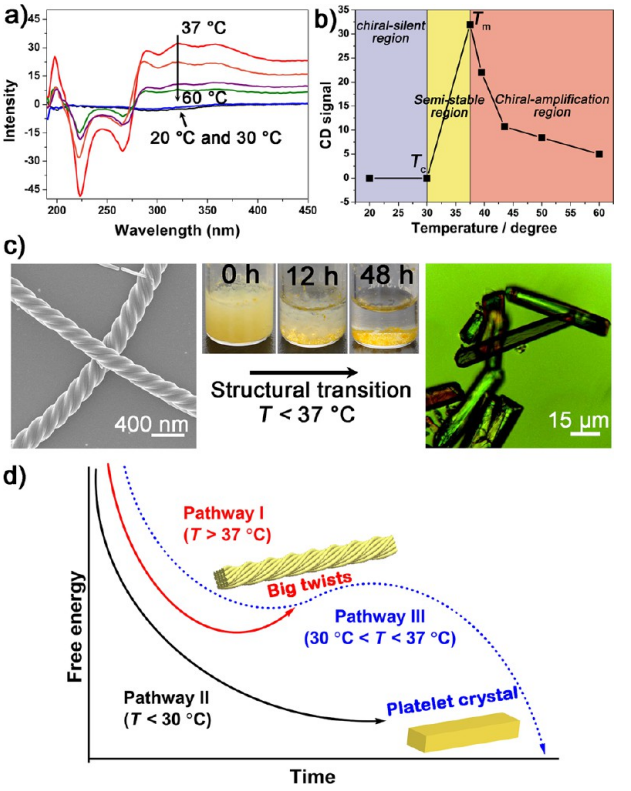

Figure 3. (a) Circular dichroism (CD) of the samples prepared at different temperatures. To avoid any semistable structures, the samples were incubated for 48 h before the CD analysis. (b) Profile of the CD intensity at 322 nm as a function of temperature. From the profile, we can define two important temperatures, T_c and T_m, which divide the diagram into three regions: a chiral-silent region ($T < T_c$), a semistable region ($T_c < T < T_m$), and a chiral-amplification region ($T > T_m$). (c) SEM, photographic, and optical microscopy images showing the structural transition of Fc-FF big twists into large crystals with the increase in incubation time at T < 37 °C. (d) Schematic diagram showing the kinetically controlled self-assembly of Fc-FF depending on temperature.

heated the crystal suspension back to T > 37 °C, then the crystals would not disrupt or reversibly transform into the big twists, indicating that the crystals were much more stable than the chiral nanostructures. The influence of temperature on the chiral self-assembly of Fc-FF reminds us that the formation of big twists is a kinetically controlled process. Figure 3d illustrates the distinct self-assembly pathway of Fc-FF depending on temperature. At T > 37 °C, Fc-FF will undergo rapid self-assembly to form elegant big twists under kinetic control (pathway I). At T < 30 °C, the loss of kinetic control arising from the slow self-assembly speed gives rise to dendritic microcrystals after 12 h of incubation (pathway II). In the semistable region, the initially formed big twists were unstable and transformed into thermodynamically stable large crystals after 1–3 days of incubation (pathway III).

The kinetic control over the formation of well-defined chiral nanostructures can be attributed to the chiral arrangement of the Fc moieties and the aromatic rings on the surface of an isolated twisted β sheet (Figure 2d). This arrangement will give rise to chiral interactions attributed to the π–π stacking and hydrophobic interactions between the sheets. Moreover, the chiral interactions will become much stronger at higher temperatures because of the increase in hydrophobic

DOI: 10.1021/jacs.5b03925
J. Am. Chem. Soc. 2015, 137, 7869–7880

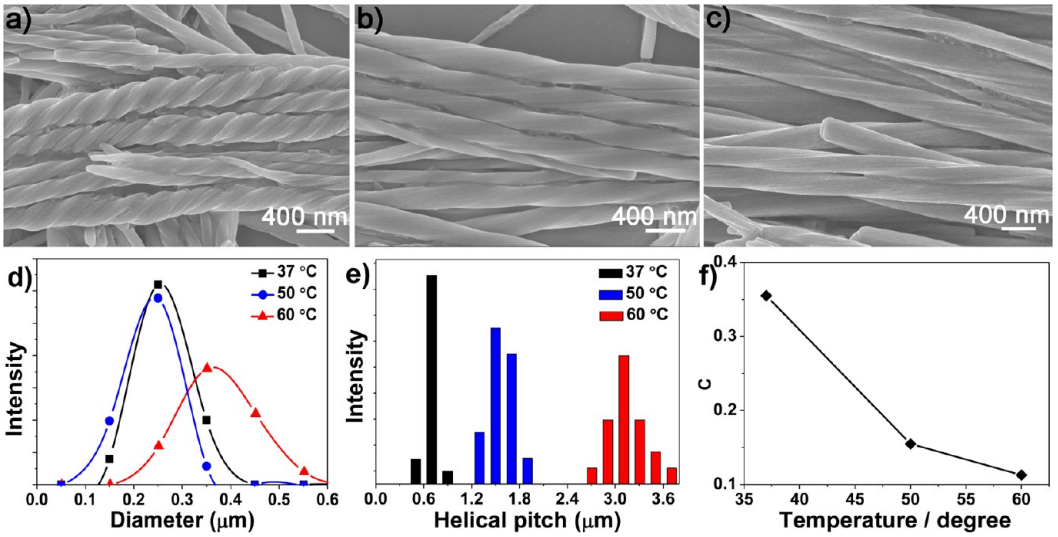

Figure 4. (a–c) Typical SEM images of the big twists formed at different temperatures: 37 °C (a), 50 °C (b) and 60 °C (c). (d and e) Diameter (D) and helical pitch (H) distributions of the big twists formed at different temperatures. (f) Profile of the C values as a function of temperature, where $C=D/H$.

interactions as temperature increases. As a result, when self-assembly proceeds at relatively low temperatures, where the chiral interactions are very weak and the self-assembling speed is very slow, the β sheets will self-assemble under complete thermodynamic equilibrium and thus are parallel-stacked with other sheets via precisely programmed "steric zipper" interactions that form platelet structures, such as dendritic microcrystals or a single crystal. However, if self-assembly proceeds at higher temperatures, where the self-assembling speed becomes very fast, then the strong chiral interactions and the emergence of molecular offsets and mispacking between the sheets will drive the helical twist of the β sheets into well-defined chiral nanostructures.

At $T > T_m$, the decrease in the CD intensity with increasing temperature suggests a synchronized structural change in the self-assembled chiral nanostructures. With this speculation, we carefully examined the SEM images in Figures 4a–c and S10c–f and discovered that the diameter (D) and helical pitch (H) of the big twists followed distinct relationships with increases in the temperature. As shown in Figure 4d, the big twists formed at specific temperatures were very homogeneous and had very narrow D distributions. The values of D remained nearly constant at 250 nm when we increased the temperature from 37 to 50 °C and only slightly increased to 350 nm when the temperature was further increased up to 60 °C. This is in sharp contrast to the self-assembly by Fc-FF alone, which lead to the formation of very thick rectangular microtubes (diameters up to tens of micrometers) at temperatures up to 37 °C (Figure S12). The thicker diameters of the platelet microstructures at higher temperatures can be attributed to the increased hydrophobic interactions, which facilitate β sheet stacking.

Compared with the response of the diameter, the H of the big twists was much more sensitive to temperature. As shown in Figure 4e, the average H of the big twists formed at 37 °C was 600–700 nm. However, with an increase in temperature, H increased to 1.6 μm at 50 °C and then to 3.1 μm at 60 °C. These results indicate that the H of the big twists could be precisely controlled through a subtle modulation of temperature. Moreover, to precisely evaluate the supramolecular chirality of the nanostructures, we defined a variable, C (the ratio between D and H), to evaluate the degree of twisting of the chiral nanostructures. The profile of the C values as a function of temperature (Figure 4f) was consistent with the profile of the CD intensity in Figure 3b.

The finite diameter and precisely controlled helical pitch of the big twists can be attributed to the competition between the gain in attraction energy (E_{attra}) associated with β sheet stacking and the elastic energy cost (E_{elast}) on the β sheets caused by the helical twist. In the theory proposed by Aggeli et al.,[15] the net energy gain, E, per peptide in a fibril, represented as

$$E = \frac{P-1}{2P}E_{attra} - E_{elast} \quad (1)$$

has a maximum at some value of P. (P is the number of ribbons in the fibril.) If we apply this theory to our system, then P can refer to the number of β sheets in the big twists. Thus, a well-defined diameter of the big twists arises, corresponding to this optimal P.

However, our system is much more complex because of the introduction of the temperature (T) variable. Because the twisted β sheets are intrinsically hydrophobic, an increase in temperature will enhance the hydrophobic interactions between the β sheets; thus, E_{attra} increases with increasing temperature:

$$E_{attra} \sim T \quad (2)$$

Moreover, by applying the theory proposed by Aggeli et al.,[15] the elastic energy cost follows:

$$E_{elast} = \frac{1}{2}k_{bend}(\nu - \nu_0)^2 + \frac{1}{2}k_{twist}(\theta - \theta_0)^2 \quad (3)$$

where ν and θ are the local curvature and the local twist strength of the β sheet within the big twists, respectively; $\nu_0 = 0$ is the equilibrium bend strength; $\theta_0 = (2\pi)/h_{\beta sheet}$ is the equilibrium value of the twist strength of an isolated β sheet; and k_{bend} and k_{twist} are the β sheet elastic constants. When we increase T, the increase in hydrophobic interactions will lead to a more compact stacking between the neighboring peptide molecules and an increase in rigidity of the β sheets. Thus, the values of k_{bend} and k_{twist} increase. E_{elast} is closely related not only

DOI: 10.1021/jacs.5b03925
J. Am. Chem. Soc. 2015, 137, 7869–7880

to the diameter (D) and helical pitch (H) of the big twists but also to the temperature (T):

$$E_{elast} \sim \psi(D, H, T) \quad (4)$$

Thus, the value of E_{elast} increases with increases in D and T and decreases with increases in H.

On the basis of eqs 1, 2, and 4, we propose that when the big twists are prepared at higher temperatures, both E_{attra} and E_{elast} increase, with the E_{elast} increasing much more intensely as a result of the increase in k_{bend} and k_{twist}. Therefore, for a maximum net energy gain E, D must increase very little as temperature increases. Moreover, the large elastic energy cost (E_{elast}) has to be released by decreasing the degree of twisting of the chiral nanostructures, which explains why the increase in temperature lead to an increase in H.

Strategy 3: Solvent-Driven, Chiral-Interaction Inversion for the Rational Design of Chiral Nanostructures with Inverted Handedness and Precisely Tailored Diameters. The modulation of solvents has always been a simple strategy to control the hierarchical self-assembly of peptides. During the fibrillization of Fc-FF, water molecules are essential for the formation of well-defined chiral nanostructures because they can form hydrogel bonds with Fc-FF to stabilize the helical architecture of the β sheets (Figure 2d,e). To trigger the self-assembly process, Fc-FF was first dissolved in organic solvent (good solvent) at high concentrations and then diluted into ddH_2O (poor solvent) to yield a mixture of 10% organic solvent and 90% H_2O (v/v). We show that very subtle modulations in the organic solvent allowed us to control the hierarchical chiral self-assembly of Fc-FF on a wide range of scales with simultaneous inversion of the supramolecular chirality. Table S1 illustrates the solvents, arranged in order of increasing polarity index. Figures 5 and S13 show SEM images of various chiral nanostructures grown under different solvent conditions (37 °C, 20 mM piperazine, pH 5.6). Intriguingly, Fc-FF self-assembled into twisted ribbons possessing an unexpected right-handed twist in 10% 2-propanol/90% H_2O (Figures 5a and S13a), whereas a slight increase in solvent polarity drives the formation of both right- and left-handed twists simultaneously in 10% methanol and 90% H_2O (Figure S13c). Moreover, with the further increase in solvent polarity, twisted ribbons or big twists possessing a homogeneously left-handed twist were formed in 10% acetonitrile/90% H_2O and 10% HFIP/90% H_2O (Figures 5b,c and S13d,f). Two strands of the left-handed big twists would sometimes be further twisted with each other in a right-handed fashion in 10% HFIP/90% H_2O, leading to the formation of a thick rope with a diameter of ~1 μm (Figure 5d). CD further explored this phenomenon. In Figure 6a, the right-handed twisted ribbons formed in 10% 2-propanol/90% H_2O (black curve and arrows) had Cotton effects completely opposite those of the big twists both in the peptide and aromatic regions (red curve and arrows), indicative of the completely molecular chiral-interaction inversion between the two chiral nanostructures. Interestingly, self-assembly of Fc-FF in 10% methanol and 90% H_2O only has very weak Cotton effects both in the peptide and aromatic regions (dark-yellow curve), possibly because of the formation of a racemic mixture of the right- and left-handed twists that is almost macroscopically CD-silent (Figure S13c). The handedness or chiral inversion that occurred with the continuous increase in solvent polarity is fascinating because in most cases left-handed chiral nanostructures should be formed from the self-assembly of peptides composed of (S) amino acids. Handedness inversion

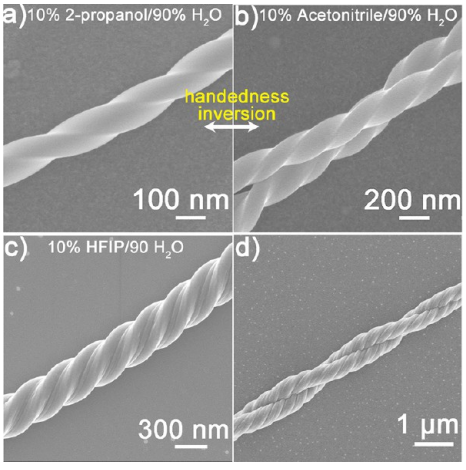

Figure 5. SEM images showing the right-handed twisted ribbons, left-handed twisted ribbons, big twists, and a right-handed rope, respectively, formed in the presence of piperazine counterions at 37 °C and pH 5.6 under different solvent conditions: (a) 10% 2-propanol/90% H_2O, (b) 10% acetonitrile/90% H_2O, and (c and d) 10% HFIP/90% H_2O.

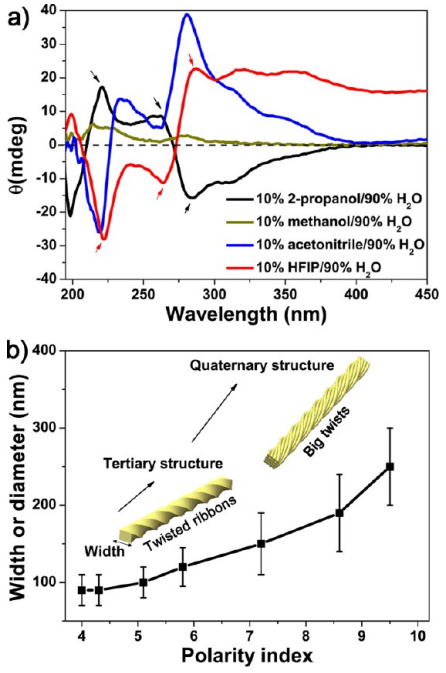

Figure 6. (a) Circular dichroism (CD) analysis of the various chiral nanostructures: right-handed twisted ribbons (black curve), left-handed twisted ribbons (blue curve), and left-handed big twists (red curve). Fc-FF will self-assemble into a racemic mixture of the right- and left-handed twists, which is almost macroscopically CD silent in 10% methanol and 90% H_2O (dark yellow curve). (b) Width or diameter distributions of the chiral nanostructures as a function of polarity index of the organic solvents (black curve). The twisted ribbons self-assembled in lower polarity solvents had a rectangular cross section and a smoothed-out surface and were self-assembled by the direct helical twisting of the β sheet. We defined these twisted ribbons as the tertiary structure. The big twists were composed of bundles of twisted ribbons and are thus the quaternary structure.

DOI: 10.1021/jacs.5b03925
J. Am. Chem. Soc. 2015, 137, 7869−7880

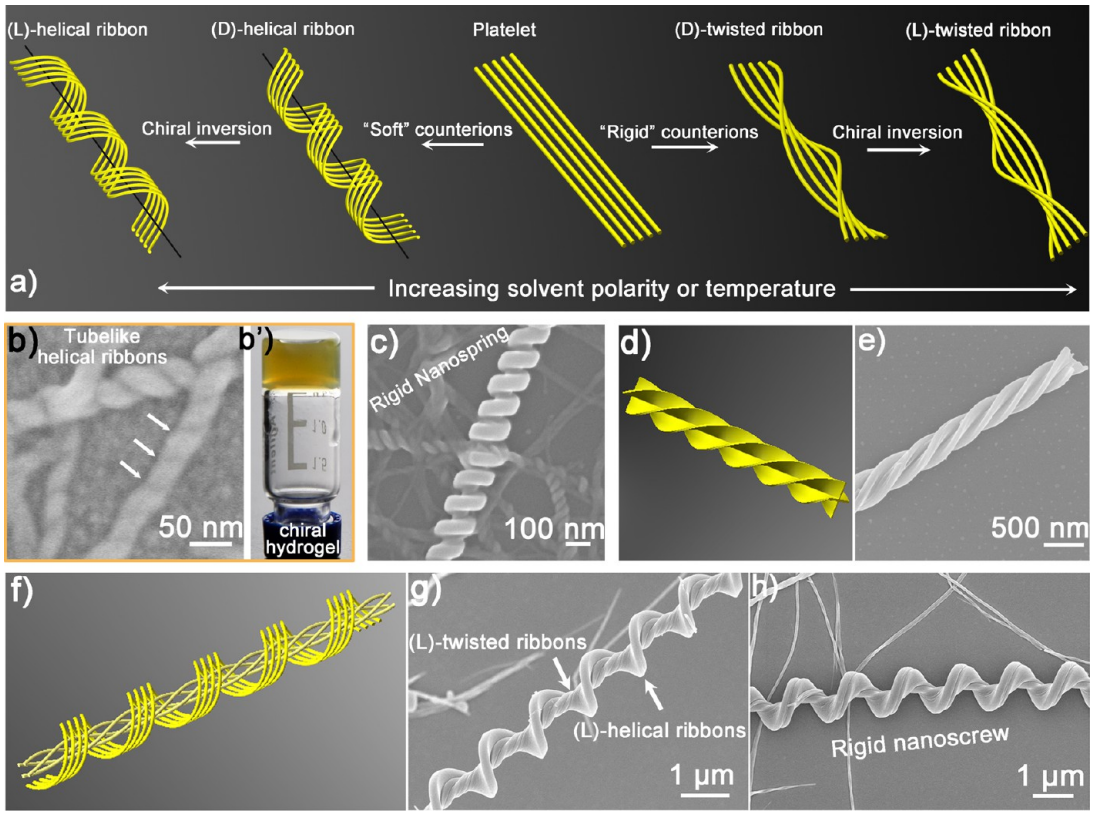

Figure 7. Rationally designed, hierarchical chiral nanostructures. (a) Generic pathway for the hierarchical chiral self-assembly of Fc-FF. Each of the yellow wires represents a simplified strand of a β sheet. Five strands of β sheets were used as models to illustrate the distinct organizational states of the β sheets. We identified two elementary forms for the helical twisting of β sheets: twisted β sheets (twisted ribbons) and helical β sheets (helical ribbons). The handedness of both could be inverted from right to left by slightly increasing the solvent polarity or temperature. (b) SEM image of the tubelike helical ribbons from the self-assembly of 4 mM Fc-FF in 10% 2-propanol and 90% PBS solution (100 mM, pH 5.6). The white arrows indicate the closed periodicity of the helical ribbons. (b′) Photographic image showing the formation of a transparent chiral hydrogel in an inverted glass vial. (c) SEM image of an elegant nanospring formed in 10% 2-propanol and 90% H_2O (20 mM ethylenediamine, pH 5.6) at 37 °C. (d) 3D model and (e) SEM image of an elegant nanohelix formed through the helical twisting of two crossed ribbons in 10% HFIP and 90% H_2O (20 mM piperazine, pH 6.0) at T = 37 °C. (f) 3D model and (g and h) SEM images showing the hierarchical architecture of the nanoscrews formed through a combination of the two elementary forms of β-sheet arrangement in 10% acetonitrile and 90% H_2O (20 mM piperazine, pH 5.6) at T = 50 °C.

during either pH changes or fibrillization progressing from self-assembly of proteins or polypeptides has been shown in several recent reports.[17,20,58] However, our results are the first example of nanostructure handedness based on the self-assembly of a short dipeptide that can be easily inversed through a slight change in solvent. This handedness inversion was also synchronized with the molecular chiral-interaction inversion, as demonstrated in the CD spectrum. A combination of IR and X-ray diffraction (Figure S14) showed that all of these chiral nanostructures had identical adsorption properties and reflection patterns, indicating very similar structural motifs among the diverse chiral nanostructures. Therefore, it is reasonable to assume that the chiral nanostructures, despite their significant morphological differences, were all formed from the hierarchical helical twisting of the peptide β sheets. However, compared with the model proposed in Figure 2d, the β sheets in the right-handed chiral nanostructures likely have the opposite handedness, as demonstrated by the CD spectrum in Figure 6a, with the Fc-FF strands rotated ~90° anticlockwise around the fiber axis.

In addition to chiral inversion, two other important features emerged with the increase in solvent polarity involved: (1) the increase in the width (W) or diameter (D) of the corresponding chiral nanostructure from 90 nm to nearly 300 nm with very narrow distributions in specific solvent conditions (Figure 6b, black curve) and (2) the levels of the hierarchical structures became much more complex and involved a stepwise amplification of molecular chirality for the chiral nanostructures assembled in higher polarity solvents (Figure 6b, insets). The increase in diameter can be explained by eq 1, where the hydrophobic interactions increase with increasing solvent polarity; thus, the gain in attraction energy (E_{attra}) increases as well, making the β sheets easier to stack into thicker bundles. However, the increase in diameter will be further restricted by the E_{elast} arising from the helical twist, which explains why the chiral nanostructures formed in a specific solvent conditions always have narrow and finite diameter distributions. The hierarchical architecture of the chiral nanostructures can also be explained by the concept of energy. It is difficult for very thick bundles of β sheets to twist all together because of the high elastic energy cost (E_{elast}) of the helical twisting of β sheets at the periphery of the bundles. Alternatively, division of this process into multiple steps will be more energetically favored, where smaller bundles of β sheets first twist into thinner ribbons, which then further stack and twist with each other and form higher levels of hierarchical chiral nanostructures. As demonstrated by the SEM images (Figure 5a,b), the twisted ribbons formed in less polar solvents had a smooth outer

DOI: 10.1021/jacs.5b03925
J. Am. Chem. Soc. 2015, 137, 7869−7880

surface and were likely formed by the direct helical twisting of the β sheets, which we defined as the tertiary structure (the model in Figure 6b). The big twists (Figure 5c) showed obvious geometric frustration and were composed of bundles of twisted ribbons belonging to the quaternary structure.

Combination of the Basic Strategies: Hierarchical, Chiral Nanostructures with Varied Forms and the Corresponding Phase Diagrams. We have demonstrated that counterions can be used to direct the chiral self-assembly of Fc-FF, and modulations in the temperature and solvent allow us to precisely control the diameter, helical pitch, and even the supramolecular chirality of the self-assembled chiral nanostructures. Here, we show how the combination of these basic strategies allowed us to obtain a wide variety of chiral nanostructures with rationally designed forms and architectures. Figure 7a illustrates a generic pathway for the chiral self-assembly of Fc-FF. Self-assembly by Fc-FF alone formed flat β sheets stacked parallel to each other, leading to the formation of platelet nanostructures. However, the mutation of the counterions at the C termini of the peptides drove the transition of secondary structures from flat β sheets into twisted β sheets. The chiral interactions and the kinetic control ultimately formed well-defined chiral nanostructures. In this process, on the basis of our systematic experimental investigations, we identified two elementary forms for the helical twisting of β sheets. (1) In the presence of rigid counterions, such as piperazine, the elementary form of the helical twisting of β sheets consisted of a twisted β sheet with a saddlelike curvature that lead to the formation of twisted ribbons. The chiral nanostructures discussed in Figures 1−6 were all grown from this form. (2) In the presence of softer counterions, such as alkali metal ions (Na^+ and K^+) or linear diamines, and less polar solvents, the elementary form of the helical twisting of β sheets consisted of a helical β sheet with a cylindrical curvature. This chiral organization of β sheets led to the assembly of elegant helical ribbons. For example, Fc-FF will self-assemble into right-handed, tubelike helical ribbons with closed periodicity in 10% 2-propanol and 90% PBS solution (100 mM, pH 5.6) at 20 °C (Figure 7b, white arrows). The tubelike ribbons were flexible, 15−40 nm in diameter, and could be entangled with each other, loading solvent molecules, which leads to the formation of a transparent chiral hydrogel (Figure 7b′). The mutation of Na^+ or K^+ ions played a crucial role in directing the chiral self-assembly of such tubelike helical structures. Self-assembly by Fc-FF alone also formed a translucent hydrogel in 10% 2-propanol and 90% ddH_2O (Figure S15a) with distinct CD properties (Figure S15b) and no chiral nanostructures within the gel (Figure S15c). In addition to the tubelike helical ribbons, more rigid and thick helical ribbons could be further assembled by changing the counterions. As shown in Figure 7c, elegant nanosprings with diameters of 100 nm and helical pitches of 150 nm were formed in the presence of ethylenediamine counterions in 10% 2-propanol and 90% H_2O at pH 5.6 and 37 °C.

We further observed the formation of much more complex chiral nanostructures by combining the elementary forms under precisely controlled self-assembly conditions (Figure 7d−h). As shown in the 3D model illustrated in Figure 7d and the SEM image in Figure 7e, elegant nanohelices can be formed through the helical twisting of two crossed ribbons in 10% HFIP and 90% H_2O (20 mM piperazine, pH 6.0) at T = 37 °C. Moreover, the initially formed twisted nanohelices nucleated the helical growth of ribbons around its outer surface in 10% acetonitrile and 90% H_2O (20 mM piperazine, pH 5.6) at T = 50 °C, which ultimately formed well-defined nanoscrews (Figure 7f−h).

We formulated two phase diagrams for the hierarchical chiral self-assembly of Fc-FF. Figure 8a illustrates the five regions

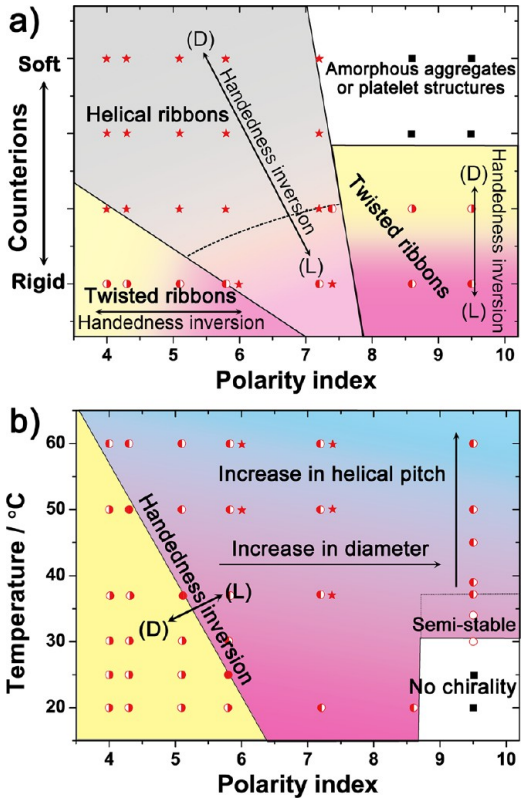

Figure 8. (a) Phase diagram for the chiral self-assembly of Fc-FF based on changes in counterions and solvent polarity. (b) Practical "handbook" for the rational control of the architecture (i.e., diameter, helical pitch, and handedness) of the self-assembled chiral nanostructures. Right- and left-filled circles correspond to D- and L-twisted ribbons, respectively; filled circles correspond to a racemic mixture of the D- and L-twisted ribbons; white-filled circles correspond to semistable twisted ribbons; red stars represent helical ribbons; and black squares represent amorphous aggregates or platelet structures.

representing distinct forms for the chiral self-assembly of Fc-FF on the basis of changes in the counterions and solvent polarity: (1) In the presence of rigid counterions and less polar solvents, twisted ribbons with right-handedness will form (yellow region, right-filled circles). However, chiral inversion from right-handedness (D) to left-handedness (L) will be observed in this region because of a slight increase in solvent polarity (region with gradient colors from yellow to pink, left-filled circles). (2) In the presence of soft counterions and less polar solvents (gray region, red stars), helical ribbons with right-handedness are the preferred form. (3) In the presence of rigid counterions and moderately polar solvents, both twisted and helical ribbons with left-handedness will form (light-pink region, red stars and left-filled circles). (4) In higher polarity solvents, the twisted ribbons with left-handedness will form in the presence of rigid counterions (pink region, left-filled circles). However, the handedness will invert when a relatively softer counterion is used (region with gradient colors from pink to yellow, right-filled circles). (5) Finally, in the presence of very soft counterions but in relatively high polarity solvents

DOI: 10.1021/jacs.5b03925
J. Am. Chem. Soc. 2015, 137, 7869−7880

(white region, black squares), amorphous aggregates or platelet nanostructures will form rather than chiral nanostructures.

Compared with Figure 8a, which primarily describes the elementary organization states of the β sheets, Figure 8b provides a more practical "handbook" for the rational control of the architecture (i.e., handedness, diameter, and helical pitch) of the self-assembled chiral nanostructures, which is formulated on the basis of the hierarchical chiral self-assembly of Fc-FF in the presence of piperazine counterions at pH 5.6. We identified three regions corresponding to distinct features for structural manipulation: (1) At lower solvent polarity and temperatures (yellow region, right-filled circles), stable right-handed chiral nanostructures will form. However, in addition to solvent, the increase in temperature will also drive the handedness inversion from right to left. For example, Fc-FF will self-assemble into D-twisted ribbons in 10% 2-propanol and 90% H_2O at 37 °C (Figure S16a), whereas L-twisted ribbons with thicker diameters will form at 60 °C (Figure S16b). (2) At higher solvent polarity and lower temperatures, no chiral nanostructures will form (white region, black squares). (3) However, left-handed chiral nanostructures will assemble at $T > 37$ °C (region with gradient colors from pink to blue, left-filled circles). As indicated by the arrows in this region, the diameter and helical pitch of the chiral nanostructures can be precisely controlled through subtle modulations in the temperature and solvent polarity.

Biological Implications and Potential Applications. In biology, counterions play a crucial role in sustaining the functions of biomacromolecules, including proteins, enzymes and DNA. The binding of counterions to a biomacromolecule changes both its conformation and biological functions. A well-known example is Na^+,K^+-adenosine triphosphatase (ATPase).[59,60] The large conformational changes of this enzyme upon binding to K^+ and Na^+ transforms the functions of ATPase that are essential for the exchange of K^+ and Na^+ across the plasma membrane. Another more relevant example is protein amyloidosis, where Cu^{2+}, Zn^{2+}, and Fe^{3+} promote the aggregation and direct the self-assembly of proteins that are involved with several neurodegenerative pathologies, such as Alzheimer's disease.[61] In our work, the incorporation of counterions during the hierarchical self-assembly of Fc-FF was a prerequisite for the formation of well-defined chiral nanostructures. The mutation of counterions at the C termini of peptides changes the secondary structures from antiparallel β sheets to twisted β sheets, thus imparting novel functions to the self-assembled materials. In this case, a strand of a β sheet can be viewed as a linear supramolecule composed of noncovalently bonded Fc-FF monomers. A change in the supramolecular conformation from an antiparallel β sheet to a twisted β sheet suggests that the effect of counterions on biomacromolecules is also applicable to small self-assembling peptides and the self-assembled supramolecular structures.

The optimized temperature (T_m) for the chiral self-assembly of Fc-FF was 37 °C (Figure 3b), which is consistent with the temperature of the human body. We believe that this is not simply a coincidence because of the large number of chiral architectures in the human body, such as DNA double helices and protein α helices. From a thermodynamic standpoint, the Gibbs free energy change (ΔG) of the diverse interacting biological systems often shows a negative minimum at approximately 37 °C.[62] Additionally, the assembly of functional architectures in biological systems is often a kinetically controlled process.[63] During the chiral self-assembly of Fc-FF, the formation of well-defined chiral nanostructures was very complex and determined by the molecular structure of the building blocks, mutation of counterions, kinetic trapping, and competition between the chiral interactions and the geometric constraints (hydrophobic interactions). The complex balance of forces from the molecular scale to the nanoscale in the chiral self-assembly of Fc-FF results in characteristic biomacromolecular interactions and a negative minimum of ΔG at 37 °C (Figure 9).

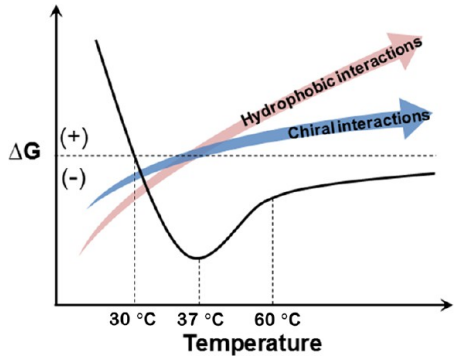

Figure 9. Conjectural plot of the Gibbs free energy change (ΔG, black curve) as a function of temperature for the chiral self-assembly of Fc-FF in 10% HFIP and 90% H_2O. Chiral nanostructures are not favored at lower temperatures ($T < 30$ °C) because of the positive value of ΔG. With an increase in temperature ($T > 30$ °C), the ΔG for chiral self-assembly became negative, with a minimum at 37 °C, and well-defined chiral nanostructures were formed. A further increase in temperature would change the balance of forces (e.g., chiral interactions and hydrophobic interactions) and slightly increase ΔG, forming less-twisted chiral nanostructures with longer helical pitches (H).

Compared to other self-assembling peptides, Fc-FF is appealing for several reasons: (1) It is difficult to amplify the chirality of smaller peptide molecules because this chirality could be easily offset when adjusting the orientation or spatial arrangement between neighboring molecules. Our results provide a feasible approach to regulate this and, by extension, other self-assembling peptides to form diverse chiral nanostructures. (2) The chiral self-assembly of Fc-FF makes this peptide an excellent probe for the chiral sensing (stereoselective recognition) of diverse diamines (Figure S17), which significantly extends the application areas of self-assembling peptides. For example, Fc-FF will self-assemble into right-handed nanohelices in the presence of (*R*)-(−)-2-methylpiperazine in 10% 2-propanol and 90% H_2O at pH 5.6, 37 °C (Figure 10a), whereas no chiral nanostructures were observed with (*S*)-(+)-2-methylpiperazine (Figure 10b). The results for the recognition of other selected chiral diamines are summarized in Table S2. Fc-FF is highly stereoselective for (*R*)-diamine enantiomers in less polar solvent (10% 2-propanol/90% H_2O), whereas it is highly stereoselective for (*S*)-diamine enantiomers in a more polar solvent (10% HFIP/90% H_2O). (For more detailed interpretations, please see the notes appended at the end of Table S2.) In 10% HFIP and 90% H_2O, the decrease in temperature will also change the effect of stereoselective recognition. These results suggest that the effect of stereoselective recognition between Fc-FF and chiral diamines can be inversed or modulated by a slight change in solvent and temperature, which can be related to the solvent- or temperature-driven chiral-interaction inversion during the hierarchically chiral self-assembly of Fc-FF. Furthermore, the

DOI: 10.1021/jacs.5b03925
J. Am. Chem. Soc. 2015, 137, 7869−7880

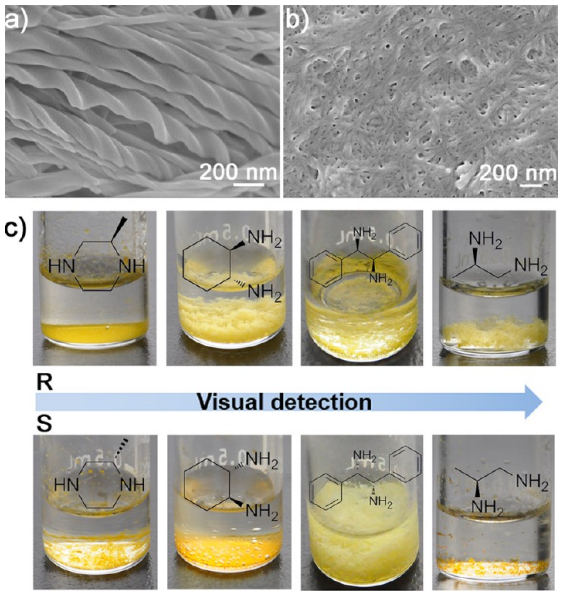

Figure 10. Formation of chiral nanostructures depending on the chirality of the counterions: (a) right-handed nanohelices and (b) nanofibers in the presence of (*R*)-(−)-2-methylpiperazine and (*S*)-(+)-2-methylpiperazine, respectively, in 10% 2-propanol/90% H_2O at pH 5.6, 37 °C. (c) Visual detection of the chiral diamines on the basis of the hierarchical self-assembly of Fc-FF. The molecular structures of different diamine enantiomers are overlaid on the corresponding photographic images.

different self-assembly behaviors of Fc-FF with different enantiomers (Figures S18−S21) will generate distinct macroscopic phenomena that can be distinguished by the naked eye, which makes visual detection of the chiral diamines possible (Figure 10c). More importantly, the enantioselective crystallization of Fc-FF with the chiral diamines (Figures S18, S20, and S21) suggests that Fc-FF may serve as a feasible resolving agent to obtain pure enantiomers by preferential crystallization.[64] (3) Finally, the Fc moiety is a redox-active site and has multiple functions. The rigid Fc-FF chiral nanostructures with tunable diameters, helical pitches, handedness, and shapes have significant potential in electrochemical sensing, asymmetric catalysis, chiroptics, or as templates for the fabrication of other chiral nanostructures, which will be the subject of forthcoming reports.

CONCLUSIONS

The precise expression of the molecular chirality of ferrocene-L-Phe-L-Phe-COOH (Fc-FF) leads to the formation of a wide variety of chiral nanostructures with finely tailored architectures. We proposed three facile strategies that provided chiral control at different stages of the peptide self-assembly: (1) The incorporation of counterions between Fc-FF β sheets leads to secondary structural mutation of antiparallel β sheets into twisted β sheets. X-ray analysis revealed that each Fc-FF strand in the sheet rotated ∼90° clockwise or anticlockwise (chiral inversion) around the fiber axis and extended via hydrogen bonding and $\pi-\pi$ stacking. (2) Increasing temperature drives the helical twisting of the sheets into well-defined chiral nanostructures under kinetic control, and decreasing temperature leads to the assembly of platelet nanostructures or a single crystal. Subtle modulations of the temperature precisely controlled the diameter, degree of twisting, and handedness of the self-assembled chiral nanostructures. (3) The solvent polarity drives the chiral-interaction inversion and increases the hydrophobic interactions between Fc-FF molecules; thus, it can be used to control the handedness and diameter of the chiral nanostructures. Through the combination of these basic strategies, we identified two elementary forms for the helical twisting of the β sheets. On the basis of these elementary forms, we created a wide variety of hierarchical chiral nanostructures: big twists, twisted ribbons, tubelike helical ribbons, nanosprings, and nanoscrews. The phase diagram of the chiral self-assembly of Fc-FF allowed us to control the diameter, helical pitch, and handedness of the self-assembled chiral nanostructures with unprecedented levels of precision. Fc-FF will serve as an archetypical template for others to use when designing new chiral self-assembling systems. Work to extend the control strategy to other self-assembling peptides and application of the chiral nanomaterials is currently in progress.

ASSOCIATED CONTENT

Supporting Information

Experimental procedures; self-assembly of ferrocene-D-Phe-D-Phe-COOH (Figure S1); Single crystal structure of Fc-FF (Figures S2−S5) and powder X-ray diffraction analysis of the rectangular nanotubes and big twists (Figure S6); SEM, CD, IR and X-ray diffraction analysis of the structures self-assembled by Fc-FF under different pH (Figure S7), counterions (Figures S8 and S9), temperature (Figures S10−S12) and solvent (Table S1 and Figures S13 and S14,); SEM and CD analysis of the Fc-FF hydrogels (Figure S15); SEM images of the temperature-driven handedness inversion (Figure S16); molecular structure of the enantiomers (Figure S17), results of stereoselective recognition (Table S2) and SEM images of assemblages formed by Fc-FF with different diamine enantiomers (Figures S18−S21). The Supporting Information is available free of charge on the ACS Publications website at DOI: 10.1021/jacs.5b03925.

AUTHOR INFORMATION

Corresponding Author

*qiwei@tju.edu.cn

Notes

The authors declare no competing financial interest.

ACKNOWLEDGMENTS

This work was supported by the Natural Science Foundation of China (nos. 21476165, 51173128, 21306134), the 863 Program of China (no. 2013AA102204), the Ministry of Science and Technology of China (no. 2012YQ090194), the Ministry of Education (no. 20130032120029), the Beiyang Young Scholar of Tianjin University (2012) and the Program of Introducing Talents of Discipline to Universities of China (no. B06006).

REFERENCES

(1) Chen, C.-L.; Zhang, P.; Rosi, N. L. *J. Am. Chem. Soc.* **2008**, *130*, 13555.

(2) Kuzyk, A.; Schreiber, R.; Fan, Z.; Pardatscher, G.; Roller, E.-M.; Hoegele, A.; Simmel, F. C.; Govorov, A. O.; Liedl, T. *Nature* **2012**, *483*, 311.

(3) Jung, S. H.; Jeon, J.; Kim, H.; Jaworski, J.; Jung, J. H. *J. Am. Chem. Soc.* **2014**, *136*, 6446.

(4) Sone, E. D.; Zubarev, E. R.; Stupp, S. I. *Angew. Chem., Int. Ed.* **2002**, *41*, 1705.

(5) Okazaki, Y.; Cheng, J.; Dedovets, D.; Kemper, G.; Delville, M.-H.; Durrieu, M.-C.; Ihara, H.; Takafuji, M.; Pouget, E.; Oda, R. *ACS Nano* **2014**, *8*, 6863.

DOI: 10.1021/jacs.5b03925
J. Am. Chem. Soc. 2015, 137, 7869−7880

(6) Cao, H.; Zhu, X.; Liu, M. *Angew. Chem., Int. Ed.* **2013**, *52*, 4122.
(7) Zou, W.; Yan, Y.; Fang, J.; Yang, Y.; Liang, J.; Deng, K.; Yao, J.; Wei, Z. *J. Am. Chem. Soc.* **2014**, *136*, 578.
(8) Chen, X.; Huang, Z.; Chen, S.-Y.; Li, K.; Yu, X.-Q.; Pu, L. *J. Am. Chem. Soc.* **2010**, *132*, 7297.
(9) Qing, G.; Shan, X.; Chen, W.; Lv, Z.; Xiong, P.; Sun, T. *Angew. Chem., Int. Ed.* **2014**, *53*, 2124.
(10) Shimomura, K.; Ikai, T.; Kanoh, S.; Yashima, E.; Maeda, K. *Nat. Chem.* **2014**, *6*, 429.
(11) Edwards, W.; Smith, D. K. *J. Am. Chem. Soc.* **2014**, *136*, 1116.
(12) Oda, R.; Huc, I.; Schmutz, M.; Candau, S. J.; MacKintosh, F. C. *Nature* **1999**, *399*, 566.
(13) Hough, L. E.; Jung, H. T.; Krueerke, D.; Heberling, M. S.; Nakata, M.; Jones, C. D.; Chen, D.; Link, D. R.; Zasadzinski, J.; Heppke, G.; Rabe, J. P.; Stocker, W.; Koerblova, E.; Walba, D. M.; Glaser, M. A.; Clark, N. A. *Science* **2009**, *325*, 456.
(14) Harper, J. D.; Lieber, C. M.; Lansbury, P. T. *Chem. Biol.* **1997**, *4*, 951.
(15) Aggeli, A.; Nyrkova, I. A.; Bell, M.; Harding, R.; Carrick, L.; McLeish, T. C. B.; Semenov, A. N.; Boden, N. *Proc. Natl. Acad. Sci. U.S.A.* **2001**, *98*, 11857.
(16) Hamley, I. W. *Angew. Chem., Int. Ed.* **2007**, *46*, 8128.
(17) Rubin, N.; Perugia, E.; Goldschmidt, M.; Fridkin, M.; Addadi, L. *J. Am. Chem. Soc.* **2008**, *130*, 4602.
(18) Adamcik, J.; Jung, J.-M.; Flakowski, J.; De Los Rios, P.; Dietler, G.; Mezzenga, R. *Nat. Nanotechnol.* **2010**, *5*, 423.
(19) Adamcik, J.; Mezzenga, R. *Soft Matter* **2011**, *7*, 5437.
(20) Usov, I.; Adamcik, J.; Mezzenga, R. *ACS Nano* **2013**, *7*, 10465.
(21) Volpatti, L. R.; Vendruscolo, M.; Dobson, C. M.; Knowles, T. P. *ACS Nano* **2013**, *7*, 10443.
(22) Fitzpatrick, A. W.; Debelouchina, G. T.; Bayro, M. J.; Clare, D. K.; Caporini, M. A.; Bajaj, V. S.; Jaroniec, C. P.; Wang, L.; Ladizhansky, V.; Müller, S. A. *Proc. Natl. Acad. Sci. U.S.A.* **2013**, *110*, 5468.
(23) Kurouski, D.; Lu, X.; Popova, L.; Wan, W.; Shanmugasundaram, M.; Stubbs, G.; Dukor, R. K.; Lednev, I. K.; Nafie, L. A. *J. Am. Chem. Soc.* **2014**, *136*, 2302.
(24) Sunde, M.; Serpell, L. C.; Bartlam, M.; Fraser, P. E.; Pepys, M. B.; Blake, C. C. *J. Mol. Biol.* **1997**, *273*, 729.
(25) Sipe, J. D.; Cohen, A. S. *J. Struct. Biol.* **2000**, *130*, 88.
(26) Nelson, R.; Sawaya, M. R.; Balbirnie, M.; Madsen, A. Ø.; Riekel, C.; Grothe, R.; Eisenberg, D. *Nature* **2005**, *435*, 773.
(27) Sawaya, M. R.; Sambashivan, S.; Nelson, R.; Ivanova, M. I.; Sievers, S. A.; Apostol, M. I.; Thompson, M. J.; Balbirnie, M.; Wiltzius, J. J.; McFarlane, H. T. *Nature* **2007**, *447*, 453.
(28) Görbitz, C. H. *Chem. Commun.* **2006**, 2332.
(29) Görbitz, C. H. *Chem.—Eur. J.* **2007**, *13*, 1022.
(30) Castelletto, V.; Hamley, I. W.; Hule, R. A.; Pochan, D. *Angew. Chem., Int. Ed.* **2009**, *48*, 2317.
(31) Adamcik, J.; Castelletto, V.; Bolisetty, S.; Hamley, I. W.; Mezzenga, R. *Angew. Chem., Int. Ed.* **2011**, *50*, 5495.
(32) Marchesan, S.; Easton, C. D.; Kushkaki, F.; Waddington, L.; Hartley, P. G. *Chem. Commun.* **2012**, *48*, 2195.
(33) Swanekamp, R. J.; DiMaio, J. T.; Bowerman, C. J.; Nilsson, B. L. *J. Am. Chem. Soc.* **2012**, *134*, 5556.
(34) Lee, N. R.; Bowerman, C. J.; Nilsson, B. L. *Biomacromolecules* **2013**, *14*, 3267.
(35) Lara, C.; Reynolds, N. P.; Berryman, J. T.; Xu, A.; Zhang, A.; Mezzenga, R. *J. Am. Chem. Soc.* **2014**, *136*, 4732.
(36) Xie, Y.; Wang, X.; Huang, R.; Qi, W.; Wang, Y.; Su, R.; He, Z. *Langmuir* **2015**, *31*, 2885.
(37) Reches, M.; Gazit, E. *Science* **2003**, *300*, 625.
(38) Kim, J.; Han, T. H.; Kim, Y. I.; Park, J. S.; Choi, J.; Churchill, D. G.; Kim, S. O.; Ihee, H. *Adv. Mater.* **2010**, *22*, 583.
(39) Huang, R.; Qi, W.; Su, R.; Zhao, J.; He, Z. *Soft Matter* **2011**, *7*, 6418.
(40) Reches, M.; Gazit, E. *Nat. Nanotechnol.* **2006**, *1*, 195.
(41) Ryu, J.; Park, C. B. *Adv. Mater.* **2008**, *20*, 3754.
(42) Song, Y.; Challa, S. R.; Medforth, C. J.; Qiu, Y.; Watt, R. K.; Peña, D.; Miller, J. E.; van Swol, F.; Shelnutt, J. A. *Chem. Commun.* **2004**, 1044.
(43) Huang, R.; Su, R.; Qi, W.; Zhao, J.; He, Z. *Nanotechnology* **2011**, *22*, 245609.
(44) Yan, X.; Li, J.; Möhwald, H. *Adv. Mater.* **2011**, *23*, 2796.
(45) Kol, N.; Adler-Abramovich, L.; Barlam, D.; Shneck, R. Z.; Gazit, E.; Rousso, I. *Nano Lett.* **2005**, *5*, 1343.
(46) Kholkin, A.; Amdursky, N.; Bdikin, I.; Gazit, E.; Rosenman, G. *ACS Nano* **2010**, *4*, 610.
(47) Gan, Z.; Wu, X.; Zhu, X.; Shen, J. *Angew. Chem., Int. Ed.* **2013**, *52*, 2055.
(48) Handelman, A.; Lavrov, S.; Kudryavtsev, A.; Khatchatouriants, A.; Rosenberg, Y.; Mishina, E.; Rosenman, G. *Adv. Optical Mater.* **2013**, *1*, 875.
(49) Yemini, M.; Reches, M.; Rishpon, J.; Gazit, E. *Nano Lett.* **2005**, *5*, 183.
(50) Jayawarna, V.; Ali, M.; Jowitt, T. A.; Miller, A. F.; Saiani, A.; Gough, J. E.; Ulijn, R. V. *Adv. Mater.* **2006**, *18*, 611.
(51) Mahler, A.; Reches, M.; Rechter, M.; Cohen, S.; Gazit, E. *Adv. Mater.* **2006**, *18*, 1365.
(52) Yang, Z.; Liang, G.; Wang, L.; Xu, B. *J. Am. Chem. Soc.* **2006**, *128*, 3038.
(53) Ikeda, M.; Tanida, T.; Yoshii, T.; Hamachi, I. *Adv. Mater.* **2011**, *23*, 2819.
(54) Wang, Y.; Huang, R.; Qi, W.; Wu, Z.; Su, R.; He, Z. *Nanotechnology* **2013**, *24*, 465603.
(55) Wang, Y.; Huang, R.; Qi, W.; Xie, Y.; Wang, M.; Su, R.; He, Z. *Small* **2015**, DOI: 10.1002/smll.201403645.
(56) Manning, M. C.; Illangasekare, M.; Woody, R. W. *Biophys. Chem.* **1988**, *31*, 77.
(57) Haris, P. I.; Chapman, D. *Biopolymers* **1995**, *37*, 251.
(58) Kurouski, D.; Lombardi, R. A.; Dukor, R. K.; Lednev, I. K.; Nafie, L. A. *Chem. Commun.* **2010**, *46*, 7154.
(59) Morth, J. P.; Pedersen, B. P.; Toustrup-Jensen, M. S.; Sørensen, T. L.-M.; Petersen, J.; Andersen, J. P.; Vilsen, B.; Nissen, P. *Nature* **2007**, *450*, 1043.
(60) Nyblom, M.; Poulsen, H.; Gourdon, P.; Reinhard, L.; Andersson, M.; Lindahl, E.; Fedosova, N.; Nissen, P. *Science* **2013**, *342*, 123.
(61) Ha, C.; Ryu, J.; Park, C. B. *Biochemistry* **2007**, *46*, 6118.
(62) Chun, P. W. *Phys. Scr.* **2005**, *2005*, 219.
(63) Dobson, C. M. *Nature* **2003**, *426*, 884.
(64) Lorenz, H.; Seidel-Morgenstern, A. *Angew. Chem., Int. Ed.* **2014**, *53*, 1218.

DOI: 10.1021/jacs.5b03925
J. Am. Chem. Soc. 2015, 137, 7869−7880